Research Article | Vol. 31, No. 4 / 13 Feb 2023 / Optics Express 6633
Optics EXPRESS

Free-running Yb:KYW dual-comb oscillator in a MOPA architecture

SANDRO L. CAMENZIND,* TOLGA SEVIM, BENJAMIN WILLENBERG, JUSTINAS PUPEIKIS, ALEXANDER NUSSBAUM-LAPPING, CHRISTOPHER R. PHILLIPS, AND URSULA KELLER

Department of Physics, Institute for Quantum Electronics, ETH Zurich, 8093 Zurich, Switzerland
*casandro@phys.ethz.ch

Abstract: Single-cavity dual-combs comprise a rapidly emerging technology platform suitable for a wide range of applications like optical ranging, equivalent time sampling, and spectroscopy. However, it remains a challenging task to develop a dual-comb system that exhibits low relative frequency fluctuations to allow for comb line resolved measurements, while simultaneously offering high average power and short pulse durations. Here we combine a passively cooled and compact dual-comb solid-state oscillator with a pair of core-pumped Yb-fiber-based amplifiers in a master-oscillator power-amplifier (MOPA) architecture. The Yb:KYW oscillator operates at 250 MHz and uses polarization multiplexing for dual-comb generation. To the best of our knowledge, this is the first demonstration of a single-cavity dual-comb based on this gain material. As the pulse timing characteristics inherent to the oscillator are preserved in the amplification process, the proposed hybrid approach leverages the benefit of both the ultra-low noise solid-state laser and the advantages inherent to fiber amplifier systems such as straight-forward power scaling. The amplifier is optimized for minimal pulse broadening while still providing significant amplification and spectral broadening. We obtain around 1 W of power per output beam with pulses then compressed down to sub-90 fs using a simple grating compressor, while no pre-chirping or other dispersion management is needed. The full-width half-maximum (FWHM) of the radio-frequency comb teeth is 700 Hz for a measurement duration of 100 ms, which is much less than the typical repetition rate difference, making this passively stable source well-suited for indefinite coherent signal averaging via computational phase tracking.

1. Introduction

The inherent stability of a periodic pulse train from a passively modelocked laser oscillator and the corresponding equidistant spacing of the comb lines in the frequency domain led to the optical frequency comb revolution [1–4]. When two similar optical frequency combs with slightly different pulse repetition rate are combined, the beating between the pulse trains in the time domain corresponds to a down-conversion of the optical comb lines down to the radio-frequency (RF) domain [5]. This unique property of dual optical frequency combs (dual-combs) makes them suitable for a wide range of applications like spectroscopy [5–8], optical ranging [9], microscopy [10] and communications [11].

For any dual-comb applications it is necessary to guarantee the stability of the two combs with respect to each other. This relative stability is determined by the relative fluctuations of the combs' line spacing, defined by the repetition rate difference Δf_{rep} and an offset on the frequency axis as defined by the carrier-envelope-offset frequency difference Δf_{CEO}. Provided that these quantities are sufficiently stable, heterodyne detection of the two optical combs yields a radio frequency spectrum consisting of discrete RF comb lines. In order to resolve these lines, their linewidth should be smaller than their spacing Δf_{rep} for a measurement time $\gg 1/\Delta f_{\text{rep}}$.

#482747
Journal © 2023
https://doi.org/10.1364/OE.482747
Received 6 Dec 2022; revised 26 Jan 2023; accepted 28 Jan 2023; published 8 Feb 2023

Optics EXPRESS

A general approach to ensure the required relative stability is to lock each comb to the same pair of narrow-linewidth continuous-wave lasers (optical references) [8,12]. This technique is powerful as it guarantees a high mutual coherence between the pair of locked frequency combs within the feedback bandwidth. However, as it relies on both stabilizing the combs' carrier envelope offset frequencies and their repetition rates it requires four individual phase locks. Despite continuous technological advances, this approach thus remains challenging and complex.

To reduce the complexity in dual-comb systems, alternative approaches exploit the fact that mode-resolved measurements only require stability of the combs relative to each other, as opposed to absolute stability. For example, by simultaneously acting on the carrier-envelope offset frequency and the repetition rate of one comb so that they follow the corresponding frequencies that define the second comb, it was possible to simultaneously synchronize Δf_{rep} and Δf_{CEO} which ensures high mutual coherence [6].

The ongoing effort to simplify dual-combs also gave rise to a new class of laser systems, the single-cavity dual-comb sources. In these single-cavity architectures, both combs share the same cavity arrangement, leading to a mutual coherence which can be sufficient for practical applications even in free-running operation without the need for fast phase-locking electronics [13,14]. Dual-comb generation from a single cavity with resolvable comb lines has been demonstrated in semiconductor disk lasers [13] and was soon followed by ring-cavity dual-comb generation schemes in free space and fiber cavities [15,16]. This paradigm shift in dual-comb laser sources resulted in the first demonstration of dual-comb spectroscopy with no further stabilization using a free-running polarization-duplexed optically-pumped semiconductor laser [17].

It is important to carefully consider the noise properties of the laser technology used in order to achieve low enough phase noise to perform coherent dual-comb measurements [18]. Typically, environmental noise sources such as vibrations dominate at low frequencies, while pump relative intensity noise (RIN) dominates at higher frequencies [19–22]. Solid-state lasers support ultra-low intensity and timing noise properties due to the cavity's low nonlinearity, dispersion, and loss [23,24], thereby mitigating RIN and other noise terms. These lasers also enable high repetition rates, substantial average powers, and near-ideal transform-limited output pulses. However, care must be taken in such solid-state lasers to mitigate environmental noise sources such as vibrations. By using a passively-cooled laser oscillator and delivering the beam through an optical fiber, the oscillator can be mechanically isolated without compromising the stability of the output beam, thereby enabling dual-comb laser deployment in noisy environments.

Modern single-mode diode modules, which fiber-deliver average powers of nearly 1 W in a narrow spectrum are appealing for pumping low-noise passively-cooled solid-state laser oscillators. However, when using one single-mode pump for both combs, dual-comb lasers have a typical output power on the order of 100 mW per comb [25,26]. While this is often sufficient, some applications such as efficient nonlinear frequency conversion to the mid-infrared benefit from watt-level average powers. Such average powers can be readily achieved by dual-comb oscillators pumped with multi-mode diode lasers, as we have recently demonstrated [14,27,28]. However, generating high power directly from the laser oscillator implies a significant thermal load and additional water-cooling circuits. This results in a more complex design to simultaneously isolate the laser from environmental perturbations, extract the heat, and maintain a stable output beam.

To address this issue, here we combine a solid-state laser pumped by a single-mode diode with a carefully designed core-pumped fiber amplifier optimized for simplicity and moderate pulse broadening in a master-oscillator power-amplifier (MOPA) architecture. The diode-pumped solid-state laser (DPSSL) exhibits a high synergy with the fiber amplifier since it is passively cooled while the amplification process can boost the output power and broaden the spectrum via self-phase modulation. At the same time, the system can benefit from the timing noise properties of DPSSLs, which are expected to be inherited by the amplified signal. Thus, the proposed MOPA architecture targets to combine the advantages of both solid-state lasers and fiber amplifiers in one modular system while maintaining minimal cooling requirements.

In the past we have explored dual-comb modelocking in cavities based on Yb:CaF_2 which support 100-fs pulses [14,26,27,29]. However, the achieved emission center wavelength was usually around 1050 nm which is not optimal for compact, high-inversion amplifiers, which exhibit higher gain at 1030 nm.

Although an efficient amplification at 1050 nm can be achieved with single- and double-clad pumped fiber amplifiers [30–32], it requires a longer active fiber to reach the same output power at this wavelength than a similar amplifier seeded at 1030 nm due to the higher gain of Yb-doped fibers at 1030 nm [31]. An increased fiber length in turn requires higher-order dispersion-optimized pulse stretching and large-scale grating compressors [30–32]. For those reasons, it is beneficial to operate the MOPA system at around 1030 nm when targeting simplicity and compactness. Operation towards 1030 nm is also beneficial for regenerative amplification for arbitrary delay scanning [33].

Here we propose a unique dual-comb MOPA configuration based on the first Yb:KYW single-cavity dual-comb oscillator in combination with a Yb-doped fiber amplifier which is significantly shorter compared to the typically several-meter-long fibers used for high-power chirped pulse amplification [30–32]. This compact and simple system emits two spatially separated pulse trains with a repetition rate of 250 MHz and a repetition rate difference continuously tunable from DC to more than 20 kHz without affecting the cavity alignment or the output beam path of the seed oscillator. This allows to modify the repetition rate difference while the laser is running. The average output power is more than 1 W per comb after the amplification process. Combined with subsequent pulse compression leading to pulse durations of 79 fs and 86 fs, this allows for efficient non-linear frequency conversion towards the mid-infrared. In addition, the sub-kHz linewidth of the RF comb over a measurement duration of 100 ms indicates that the demonstrated dual-comb architecture is suitable for free-running mode-resolved measurements such as dual-comb spectroscopy.

2. Single-mode pumped Yb:KYW oscillator

Yb-doped double-tungstate gain materials (Yb:KGW and Yb:KYW) are well established for modelocked lasers [34–40]. These biaxial crystals have favorable optical properties for femtosecond modelocking with low-power pump diodes, including a high nonlinear coefficient, a broad emission spectrum, and a relatively short upper state lifetime. With N_g-cut Yb:KYW, both polarization states (polarization along the N_m- and N_p-direction) have a large emission cross section, and the N_m-direction has a high pump absorption cross section. The gain peak for both polarizations is close to that of Yb-doped fibers when they are operated at high population inversion, which will allow for use of very short amplification fibers with no need for chirped pulse amplification if the oscillator's pulse repetition rate is sufficiently high. These considerations make Yb:KYW an interesting and as-yet unexplored candidate for dual-comb modelocking.

The 250-MHz laser oscillator is based on a folded end-pumped cavity supporting two cross-polarized laser modes simultaneously as shown in Fig. 1(a). The 2-mm long N_g-cut Yb:KYW gain crystal (5% doping concentration) is pumped through a flat output coupler with a transmission of 2.6% for the laser wavelength and high transmission for the pump wavelength. The gain crystal is wedged to avoid etalon effects and has an anti-reflection (AR) coating for wavelengths between 975 nm and 1070 nm to avoid losses for the pump and laser wavelength. The pump is a 980-nm wavelength-stabilized single-mode pump-diode (1999CVB, 3SP Technologies) driven by the CTL300E, Koheron. To maximize the pump-induced noise correlations between the two cross-polarized laser modes, we split the collimated pump beam into two beams of equal power using a plate beam splitter and then recombine them with a small spatial separation using a D-shaped mirror. The two parallel rays are then imaged into the gain crystal with a pair of lenses.

Optics EXPRESS

The resulting focused pump spots are separated spatially by about 270 μm in the gain crystal. It is critical to pump each mode independently to avoid gain cross-talk. The polarization of the linearly polarized pump light is adjusted to the N_m-axis of the Yb:KYW crystal using a half-wave plate to maximize its absorption. Directly behind the gain crystal, the two cross-polarized intracavity modes are combined using a 5-mm long wedged birefringent $CaCO_3$ crystal so that from there on the two modes can co-propagate throughout almost the complete cavity until they are separated again just before the cavity end mirror. We maximize the common path of the two modes to reduce their relative timing and phase noise. The cavity end mirror is a semiconductor saturable absorber mirror (SESAM) [41], which has a modulation depth of 1.25%. Before the SESAM, we split the two laser modes with a 6-mm long wedged birefringent α-BBO crystal to ensure independent saturable absorption for the two modes and to prevent saturation cross-talk. Both birefringent crystals, $CaCO_3$ and α-BBO, are cut at an angle of 45° with respect to the c-axis of the crystal. Since all cavity components together with the pump source are shared by the two combs, this system exhibits high intrinsic dual-comb coherence.

The $CaCO_3$ crystal and the α-BBO crystal are rotated by 90° with respect to each other around the optical axis to partially compensate for the relative delay between the ordinary and the extraordinary wave due to the spatial walk-off. The material and length of these two crystals were chosen such that the associated delay between the two cross-polarized modes cancels the delay due to the anisotropy of the group index in the Yb:KYW crystal. This ensures that the repetition rate difference Δf_{rep} between the two frequency combs can be adjusted to a value below a few kHz which is necessary to prevent aliasing effects.

The repetition rate difference can be continuously adjusted by tilting the α-BBO crystal, as this varies the optical path length difference between the two modes. As this tilt does not couple to the cavity alignment, this allows to tune the repetition rate difference from DC to more than 20 kHz by changing the tilting angle of the α-BBO crystal by approximately 5 degrees. The laser has a nominal pulse repetition rate of 250 MHz (Fig. 1(f)) and during the measurements the repetition rate difference was set to $\Delta f_{\text{rep}} = 10.8$ kHz (Fig. 1(g)).

By introducing negative group-delay dispersion (GDD) with dispersion-compensating mirrors (–2790 fs^2 per cavity roundtrip) we achieve fundamental soliton modelocking [42]. While the negative GDD introduced by the mirrors is the same for the two intracavity modes, they experience a different amount of self-phase modulation (SPM) inside the three intracavity crystals. In combination with the different gain spectra for the ordinary and extraordinary waves in the gain medium, this manifests itself in unequal pulse durations for the two resulting pulse trains. The intensity autocorrelation traces reveal 118-fs pulses for the output along the N_m-axis of the Yb:KYW gain crystal (comb 1), and 173-fs pulses along the N_p-axis (comb 2) at the highest output power (Fig. 1(b) and 1(e)). Similarly, the polarization-dependent gain spectra also lead to mismatched output powers (Fig. 1(b)) and unequal optical spectra (Fig. 1(d)) for the two combs. The emission spectrum is centered at 1040 nm (1043 nm) with a full-width half-maximum (FWHM) bandwidth of 10.2 nm (7.6 nm) for comb 1 (comb 2).

Optics EXPRESS

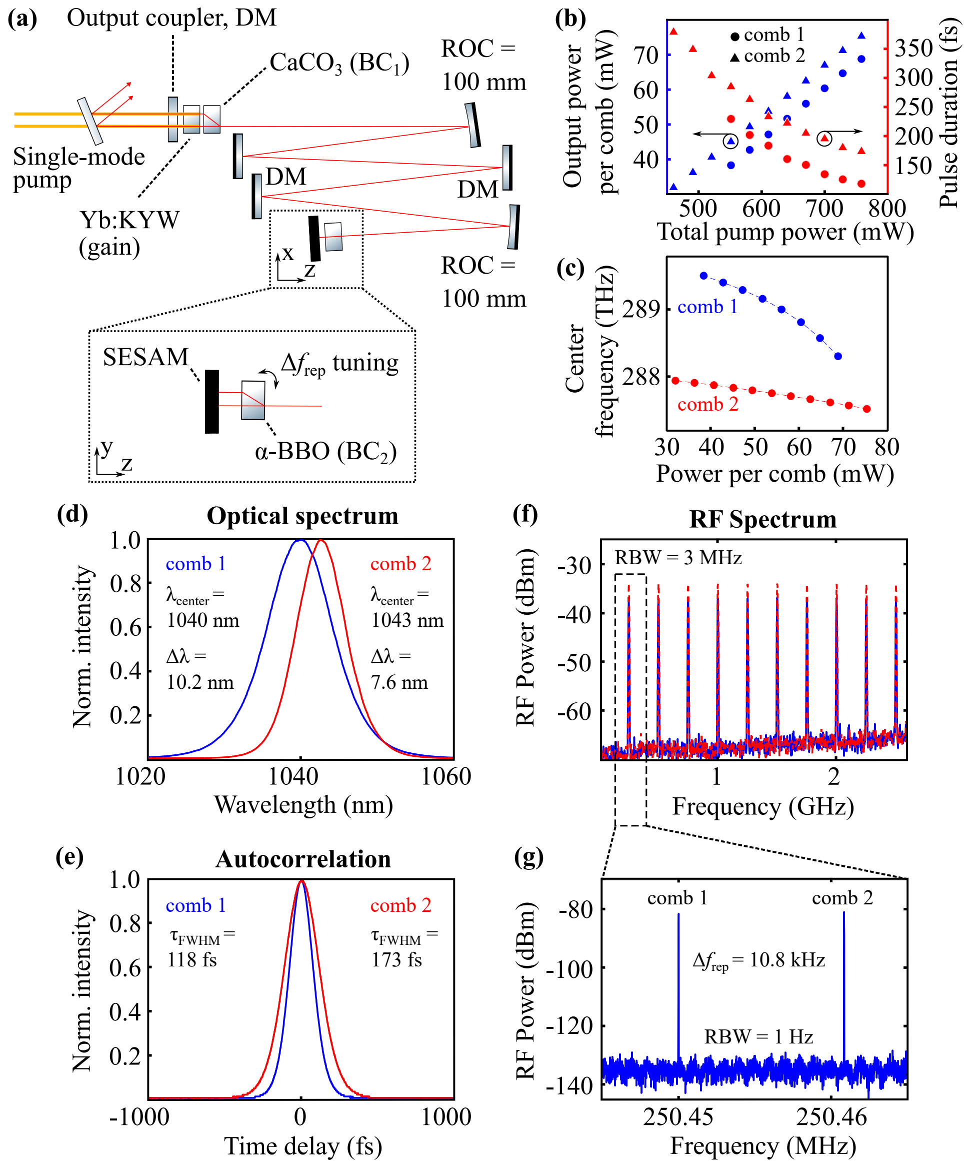

Fig. 1. (a) Schematic of the 250 MHz dual-comb Yb:KYW laser based on a common-path polarization-multiplexed cavity using a first birefringent $CaCO_3$ crystal (BC_1) to spatially separate the intracavity modes on the gain crystal and a second birefringent α-BBO crystal (BC_2) to induce spatial separation of the modes on the SESAM (DM = dispersive mirror, ROC = radius of curvature). (b)–(g) Characterization of the laser performance in simultaneous dual-comb lasing operation: (b) output power and pulse duration as a function of total pump power. The indicated pump power is split equally between the two laser modes; (c) optical center frequency as a function of output power per comb; (d) clean optical spectrum for comb 1 and comb 2; (e) intensity autocorrelation traces and corresponding pulse duration; (f) radio-frequency (RF) spectrum with (g) zoom on the first harmonic around 250 MHz (RBW = resolution bandwidth).

Optics EXPRESS

3. MOPA architecture with Yb-doped-fiber based power amplifier

The MOPA architecture consists of the single-mode pumped Yb:KYW dual-comb oscillator (Section 2) and one core-pumped Yb-doped fiber amplifier for each output beam of the oscillator as illustrated in Fig. 2(a). Each comb is first directed through a half-wave plate (HWP) and a free-space Faraday isolator (FI) to prevent back-reflections into the oscillator. After passing through another HWP for orienting the linearly polarized light, they are separately coupled into the input port of a polarization-maintaining wavelength-division multiplexer (WDM) to combine the seed with the forward-propagating pump light from a single-mode pump diode before being directed to the core-pumped Yb-doped active fiber. Although the absorption maximum of Yb-doped fibers is around 976 nm, we used a pump diode at 980 nm (1999CVB, 3SP Technologies) since this was available at the time of the project. The longer pump wavelength implies a slight reduction in the maximum population inversion achievable in the fiber, but this only has a marginal effect on the experiment. A slightly shorter gain fiber could be used with a 976-nm pump.

To support higher powers than would be provided by a single pump diode, we add a backward-propagating pump diode for bidirectional pumping. Its light is coupled into the active fiber from free-space via a dichroic mirror, which in turn allows coupling the amplified pulses directly out of the active fiber. This avoids excessive pulse broadening associated with the propagation of intense light pulses in single-mode fibers. The output tip of the active fiber is angularly cleaved (8°) to prevent amplification of the Fresnel back reflection. An additional FI enclosed by two HWPs is included between the active fiber and the backward pump to prevent the amplified dual-comb signal or light from the forward pump from damaging the backward-pump diode.

With this configuration we obtain average output powers up to more than 1 W per comb (Fig. 2(b)). While significantly higher output powers of 100 W and more would be possible with alternative configurations that employ the chirped pulse amplification scheme with several-meter-long Yb-doped fibers and rod-type photonic crystal fibers [30–32], our approach requires only a standard single-mode area fiber and no pre-chirping of the input pulses.

The active fiber has a length of 30 cm, which according to our simulations is the shortest length that still provides sufficient gain to strongly saturate the amplifier. The short fiber length ensures that the amount of dispersion and pulse broadening remains low which simplifies the pulse compression after the amplification process significantly: with only around -20’000 fs^2 of negative GDD introduced with a pair of transmission gratings in a double-pass configuration (grating period is Λ_g = 1250 lines/mm and separation between the two gratings is $L_g \approx 1.5$ mm), we compress the pulses to 79 fs (comb 1) and 86 fs (comb 2) as shown in Fig. 2(c). A HWP is used before the grating pair to align the polarization with the lines of the grating, thereby maximizing the power throughput. The total transmission efficiency through the double-pass grating pair compressor was measured to be >75%. The pulses were characterized with a frequency-resolved optical gating (FROG) (PS-700, Femto Easy) [43,44]. The flat temporal phase during the two femtosecond pulses (dashed lines in Fig. 2(c)) as well as the flat spectral phase in the wavelength region of the optical spectra (dashed lines in Fig. 2(e)) imply a successful pulse compression. As expected, the fiber amplifier also induces a significant broadening of the optical spectra to a FWHM of 31.8 nm (28.5 nm) for comb 1 (comb 2) so that they now exhibit a significant spectral overlap (Fig. 2(d) and 2(e)). To illustrate this, the dashed lines in Fig. 2(d) show the optical spectra before the amplification process.

The entire MOPA system is passively cooled which is favorable for simplicity, compactness, and portability. The architecture is also beneficial for minimizing noise at low frequencies, which is a critical consideration for successful dual-comb measurements. First, passive cooling avoids vibrations that can be introduced by active water or air cooling. Second, while our laser demonstration here was constructed on a standard optical table, the oscillator could be assembled

Optics EXPRESS

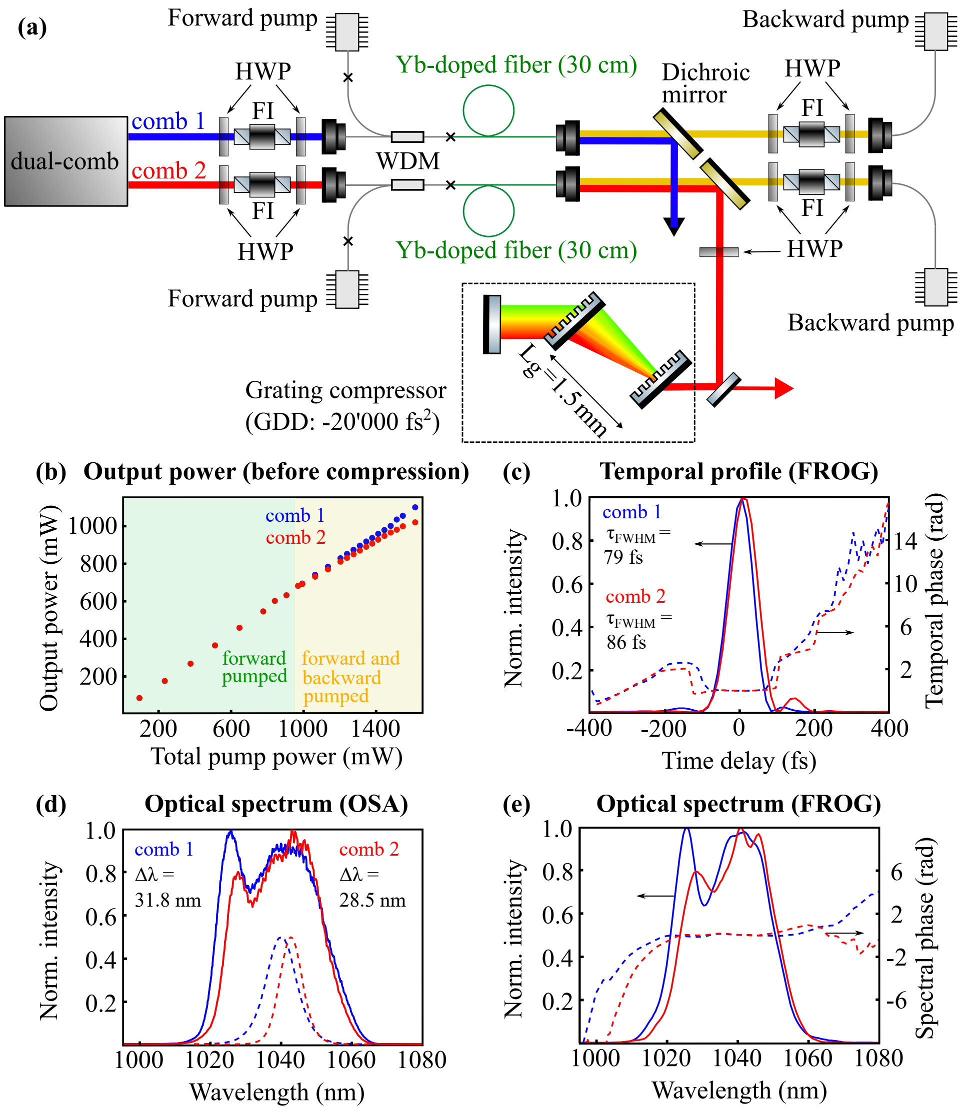

Fig. 2. (a) Schematic of the MOPA architecture consisting of a low-power dual-comb oscillator and a dual fiber amplifier. After the amplification process, the pulses are compressed with a simple grating compressor (FI = Faraday isolator, HWP = half wave plate). (b) Output power of the two combs after the amplification process but before pulse compression. In the green region, only the forward pump was used while in the yellow region both pumps were active. (c) Temporal profile of the pulses after pulse compression according to a frequency-resolved optical gating (FROG) measurement. The dashed lines describe the temporal phase. (d) Optical spectra of the cross-polarized beams before the amplification (dashed lines) and after the amplification (solid lines) as measured with an optical spectrum analyzer (OSA). (e) Optical spectrum according to a FROG measurement. The retrieved spectra are similar to the data shown in (d) which validates the FROG measurement. The dashed lines describe the spectral phase.

in a vibration isolated housing. Doing so would further improve the noise performance and allow operation in noisier environments.

Optics EXPRESS

4. Intensity and timing noise properties

To prove the usefulness of the proposed hybrid approach for dual-comb applications, we carefully studied the impact of the amplification process on the intensity and timing noise properties of the system.

It is known that fluctuations of the laser's optical center frequency induce timing noise [19–22]. Consequently, the coupling of intensity noise to timing jitter is influenced by the shift in optical center frequency due to a certain output power variation, i.e., the slope of the optical center frequency as a function of output power at the operation point of the laser.

To study the influence of one laser parameters on another, a transfer function analysis can be useful as discussed for example in [45]. The transfer function of output power to optical center frequency depends on the emission cross-section of the gain-medium, meaning that with the anisotropic gain material a qualitatively different behavior is expected for the two cross-polarized beams. For comb 2, we observe a linear relationship between output power and optical center frequency, with a slope of around -10 GHz/mW as visible from Fig. 1(c). The transfer function of comb 1 exhibits an almost linear slope up to an oscillator output power of around 50 mW where the frequency shift is approximately -30 GHz/mW (Fig. 1(c)), and an even steeper slope for higher output powers.

To minimize intensity-to-timing-noise coupling for both combs while still maintaining a sufficient output power to seed the amplifier system, we operate the dual-comb just before the point where the slope start increasing significantly for comb 1, i.e., at an output power of 48 mW (55 mW) for comb 1 (comb 2). The output power after the amplification process is around 800 mW per comb for the noise measurements.

4.1. Intensity noise properties of the MOPA architecture

A key parameter for many dual-comb applications is the RIN. From amplifier theory [46,47], it is expected that the RIN of the pump diode dominates for low frequencies as pump power fluctuations lead to population variations of the upper laser level, which directly couples to the amplifier's output power. For pump power fluctuations at high frequencies (faster than the amplifier can respond), the population of the upper laser level can no longer adapt so that in this regime the amplifier's RIN is dominated by the intensity noise of the oscillator [46,47].

For most solid-state lasers the RIN spectrum, as measured in dBc/Hz, is orders of magnitude larger at low frequencies (e.g., <1 kHz) compared to the shot noise limited values obtained at high frequencies (e.g., >1 MHz). This disparity makes it difficult to analyze the full RIN spectrum in a single measurement with high sensitivity. To circumvent this issue, we measure the RIN at low and high frequencies with a separate setup that employs different low-noise amplifiers optimized for the respective frequency domain. The resulting power spectral densities (PSDs) are stitched in the post-processing to receive a high-dynamic-range RIN measurement [14]. For the slow frequencies (<200 kHz), we amplify the electronic signal from a photodetector (DET10N2, Thorlabs) modified to handle higher optical power, with a low-noise transimpedance amplifier (DLPCA-200, Femto) before performing a baseband measurement with a signal-source-analyzer (SSA) (E5052B, Keysight). The average optical power on the photodetector was around 6 mW. For analyzing the high-frequency-noise components, the signal is first split into its AC and DC part using a bias-tee (BT45R, SHF Communication Technologies AG). The DC part is used as a reference for normalization purposes, while the AC part is amplified with a low-noise voltage amplifier (DUPVA-1-70, Femto) prior to the baseband measurement with the SSA. We analyzed the noise before and after amplification, and with/without active stabilization on the oscillator pump power. The measurement results are shown in Fig. 3. The two oscillator outputs are solid

Optics EXPRESS

lines, while the amplified outputs are dashed lines. Comb 1 and comb 2 are shown in blue and red, respectively.

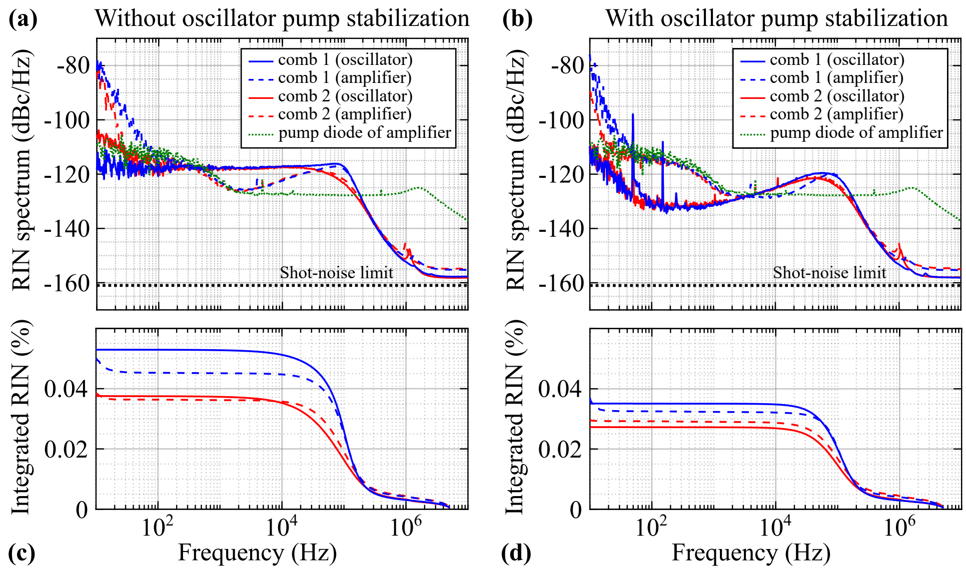

Fig. 3. One-sided relative intensity noise (RIN) power spectral density for both combs before amplification (solid line) and after amplification (dashed line) (a) without and (b) with output-power-stabilization of the oscillator's pump diode. The shot-noise limit was calculated from the photocurrent of the photodiode. (c) and (d): Corresponding integrated RIN with an upper integration frequency of 5 MHz.

For frequencies between 70 Hz and a few kHz, we find that the RIN of the amplified beams corresponds closely to the pump RIN, while for higher frequencies it approaches the RIN of the oscillator, as expected. For frequencies <70 Hz, the amplified RIN is higher for comb 1, likely due to variations of the coupling efficiency into the fiber amplifier caused by beam-pointing fluctuations of the seed and the backward-propagating pump. For frequencies >1 MHz, the increase of the amplifier's RIN can be explained by amplified spontaneous emission (ASE) which is not taken into account in the considered theoretical models describing amplifier noise transfer function theory [46,47].

To further improve the noise performance of the system, we stabilized the power of the single-mode laser diode used for pumping the oscillator. For that purpose, we spliced a polarization-maintaining 99:1 fiber-splitter directly to the output of the pump diode. The output port with 99% of the pump power was used for pumping the Yb:KYW gain crystal, while the second output port was detected with a photodiode. The resulting error signal was then used to stabilize the pump power using a PI^{2}D controller (D2-125 Laser Servo, Vescent Photonics). The resulting improvement in the RIN is shown in Fig. 3(b) and 3(d) for the two oscillator outputs (solid lines) and the corresponding signals after amplification (dashed lines).

The RIN of the oscillator output is significantly reduced for frequencies up to almost 100 kHz. The sharp peaks in the oscillator's RIN at 50 Hz and integer multiples thereof originate from the electrical power grid connected with the PI^{2}D controller. Since the amplifier's RIN is largely determined by the pump power fluctuations for frequencies up to a few kHz, these peaks are suppressed after the amplification process. For the same reason, the pump power stabilization only impacts the amplifier's RIN at frequencies beyond a few kHz leading to a reduction of the integrated RIN from 0.045% (0.036%) down to 0.033% (0.029%) for comb 1 (comb 2) when integrating from 5 MHz down to 100 Hz (Fig. 3(b) and 3(d)).

Optics EXPRESS

The oscillator's low nonlinearity, dispersion, and loss enables a low noise level of -158 dBc/Hz at high noise frequencies. This is almost 10 dB lower than the noise floor of well-documented state-of-the-art mode-locked Yb:fiber lasers [32,48,49]. The substantial power of the solid-state oscillator also enables a low noise floor of -155 dBc/Hz even after amplification. This is around 15 dB lower than the high-frequency noise level described in previous fiber-oscillator-based amplifier systems [31,32]. Compared to fiber oscillators [32,48,49], solid-state lasers are susceptible to some additional environmental noise sources such as mirror vibrations, but this issue can be addressed by integrated or monolithic laser constructions [50].

Here we are using a passively cooled laser oscillator to minimize excessive mechanical vibrations and also stabilize the power of the oscillator's pump diode. To further reduce the RIN of the amplified dual-comb at lower frequencies, one could additionally stabilize the power of the amplifier's pump diodes with the same stabilization approach already used for the oscillator's pump. However, a significant advantage of stabilizing the oscillator's pump diode is that aside from reducing the RIN, the pump power stabilization also affects the timing noise of the system as will be discussed in the next section. Since stabilizing the amplifier's pump diodes on the contrary does not affect the timing noise, we decided that the added complexity of an individual locking system for each of the four amplifier pump diodes is not sensible for this laser system.

4.2. Timing noise properties of the MOPA architecture

To characterize the repetition rate timing noise of each frequency comb, we first detect each pulse train on a fast photodetector (DSC30S, Discovery Semiconductors Inc.) and filter out the 60$^{\text{th}}$ repetition rate harmonic with a tunable bandpass filter to improve the sensitivity of the measurement after normalization to the laser repetition rate [22]. The timing jitter power spectral density (TJ-PSD) of the resulting signal is then characterized with the SSA.

To investigate the effectiveness of the common-cavity approach, we use a relative timing jitter measurement based on beating each comb with a pair of single-frequency continuous wave (cw) lasers which reveals the relative timing jitter of our free-running dual-comb system [26]. We evaluate the timing noise at a typical repetition rate difference of $\Delta f_{\text{rep}} = 10.8$ kHz (green in Fig. 4).

The timing noise of the individual combs is preserved in the amplification process (Fig. 4). The two combs exhibit, however, a qualitatively different TJ-PSD (Fig. 4(a)). The observed discrepancy originates from the gain-anisotropy experienced in the birefringent gain crystal which leads to an about three times steeper slope of the optical center frequency as a function of output power for comb 1 than for comb 2. Since both combs exhibit similar RIN spectra (Fig. 3), this factor of three is expected also in the relative strength of the combs optical center frequency fluctuations, so that the difference between the associated PSDs describing the optical center frequency fluctuations scales by this factor squared. Provided that the impact of optical center frequency fluctuations starts to dominate the timing noise of the combs for frequencies >100 Hz, this difference directly transfers to the TJ-PSD which explains the observed discrepancy of around 10 dB between the combs timing noise [19,51]. Consequently, at those noise frequencies passive noise cancellation is hardly possible so that it is not surprising that the relative TJ-PSD largely follows the curve describing the noisier comb 1 (blue). The assimilation of the combs timing noise at high offset frequencies around 100 kHz is attributed to the increasing influence of the measurement noise floor which starts to dominate.

Stabilizing the output power of the oscillator's pump diode reduces the RIN (see Section 4.1) and thereby also the timing noise due to reduced optical center frequency fluctuations. The resulting reduction of the TJ-PSD inherent to comb 1 similarly affects the relative timing noise (Fig. 4(b) and 4(d)).

At lower frequencies between 10 Hz and 1 kHz, the noise spectrum of the individual combs is dominated by prominent peaks at integer multiples of 50 Hz, that likely originate from the

Optics EXPRESS

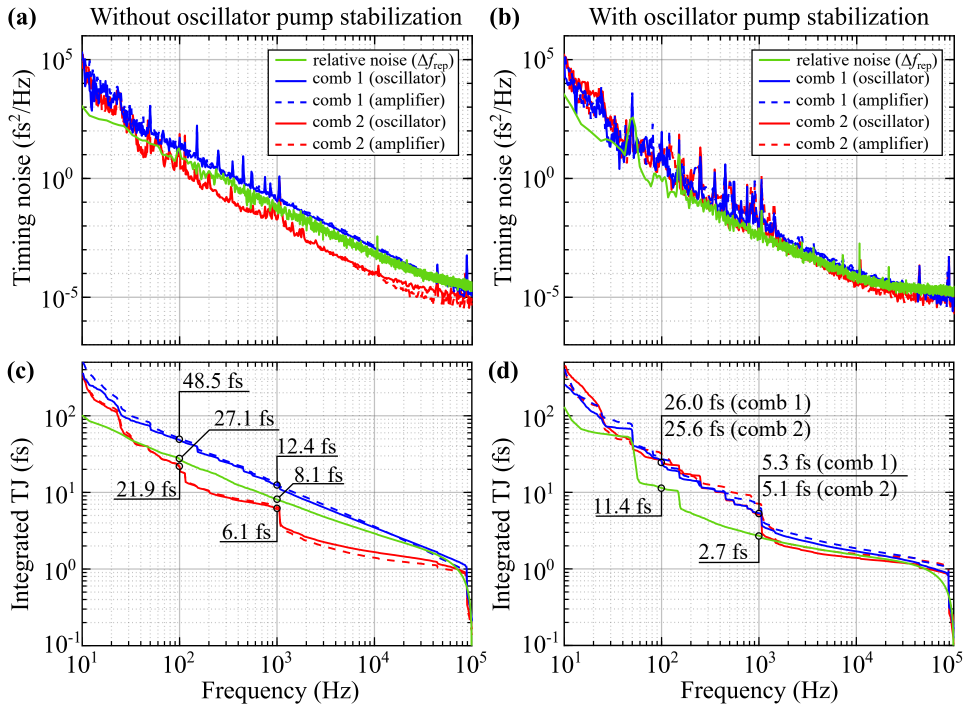

Fig. 4. One-sided timing jitter power spectral density (TJ-PSD) for both combs before amplification (solid line) and after amplification (dashed line) (a) without and (b) with output-power stabilization of the oscillator's pump diode. To enhance the readability of the figure, we applied a moving average to the relative TJ-PSD. (c) and (d): Corresponding integrated timing jitter (TJ) with an upper integration frequency of 100 kHz.

spikes caused by the PI^{2}D controller which are also visible in the RIN (see Fig. 3(b)). Due to the single-cavity architecture in which all cavity components and even most of the intracavity beam path is shared by the two combs, these peaks are present in both combs. Thus, most of them get suppressed in the relative timing noise which leads to a reduction of the integrated timing jitter from around 5 fs [1 kHz, 100 kHz] for the individual combs down to only 2.7 fs [1 kHz, 100 kHz] for the relative timing noise.

The noise of the individual combs is comparable to the noise performance of previous single-cavity dual-comb solid-state lasers with a timing jitter of around 8.7 fs [1 kHz, 100 kHz] for each comb [14]. However, due to the anisotropic gain material used in combination with birefringent multiplexing for dual-comb generation, the two combs exhibit a slightly different timing noise power spectral density leading to reduced common noise suppression compared to previous single-cavity dual-combs based on isotropic gain crystals [14].

5. Comb-line resolution

A low relative timing jitter is important for applications that rely on a high relative stability of the periodic pulse trains, for example time-of-flight based dual-comb ranging [52]. However, this parameter does not indicate the suitability of the system for applications that require comb-line resolution such as dual-comb spectroscopy. For such applications, the noise on the RF comb lines themselves is critical, and this is influenced by both Δf_{rep} and the relative carrier-envelope offset frequency Δf_{CEO}. In this section, we thus focus on the combined effect of fluctuations in the relative frequencies Δf_{CEO} and Δf_{rep} between the comb lines for the proposed dual-comb laser with stabilized oscillator pump power.

To assess the relative coherence of the laser, we determine the linewidth of a single RF comb line by heterodyning each comb with a single-frequency cw laser at 1064 nm (ORION 1064 nm Laser Module, RIO). By heterodyning the resulting RF signals digitally, the noise contribution of the cw laser cancels. Thus, we are essentially recording the beat note between one comb tooth from each comb. In the frequency domain, this signal corresponds to a single RF comb tooth of which we can extract the linewidth. This is an established technique for characterizing single-cavity dual-comb sources [16,25,53].

For a measurement duration of $\tau_{\mathrm{meas}} = 100$ ms, this technique reveals a typical FWHM linewidth of around 700 Hz. The underlying phase profile that arises from the heterodyned signals is used to determine the corresponding phase noise power spectral density. Scaling it by frequency yields the frequency noise power spectral density (FN-PSD) of an individual RF comb line, which reveals the contribution of the different noise frequencies to its linewidth via the β-separation line formalism [54]. The FN-PSD in Fig. 5(b) indicates that noise at frequencies >200 Hz (which lies below the β-separation line) does not contribute to the RF comb linewidth, i.e., only for measurement times longer than around 5 ms does the FN-PSD cause the linewidth to broaden beyond the inverse of the measurement time. According to Fig. 4(b) and 4(d), the common noise suppression of the single-cavity architecture works very well in this frequency band: even though the two combs exhibit different amplitude-to-timing noise transfer functions which makes noise suppression generally more difficult, the common cavity approach suppresses enough noise at lower frequencies (particularly noise spikes) such that a very high relative stability between the two combs can be achieved with our free-running system.

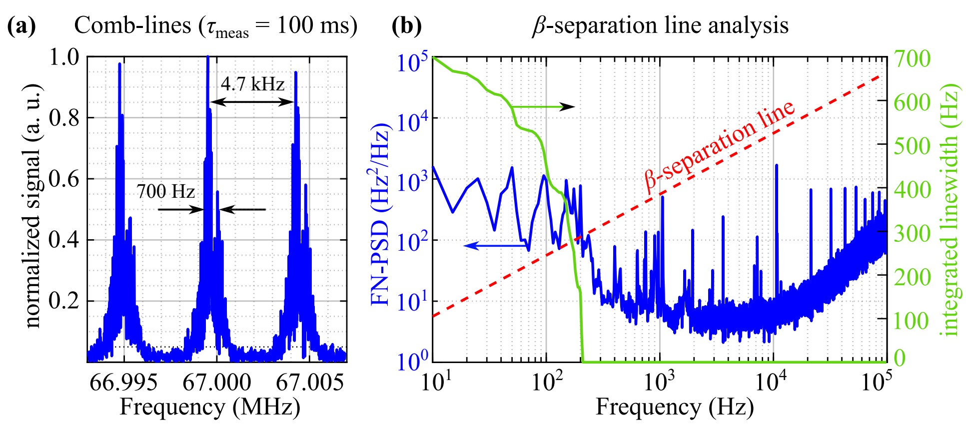

Fig. 5. Relative coherence assessment of the dual-comb laser (a) zoom into dual-comb spectrum with $\Delta f_{\mathrm{rep}} = 4.7$ kHz obtained via Fourier transformation of consecutive interferograms recorded for a measurement time of $\tau_{\mathrm{meas}} = 100$ ms. (b) Left axis: Frequency noise power spectral density (FN-PSD), together with the β-separation line. Right axis: FWHM linewidth of a single RF comb tooth corresponding to the FN-PSD according to the β-separation line formalism [54].

This suggests that the repetition rate difference can be further reduced to counteract spectral aliasing while still resolving the individual comb lines. To demonstrate this, we overlap both pulse trains with Δf_{rep} reduced to 4.7 kHz and record the resulting interferometric signal for a measurement time of $\tau_{\mathrm{meas}} = 100$ ms. This duration corresponds to almost 500 interferogram periods (one interferogram period lasts $1/\Delta f_{\mathrm{rep}} \approx 0.21$ ms). To find the dual-comb spectrum we take a Fourier transform of the raw data without any phase or timing correction. As apparent from

Optics EXPRESS

a zoom into the central part of this spectrum (Fig. 5(a)) the comb lines are still well-resolved, which indicates that comb-line resolution would be possible with even lower Δf_{rep} if necessary.

The measured RF comb linewidth of 700 Hz (τ_{meas} = 100 ms) is comparable to the linewidth of around 2 kHz (τ_{meas} = 100 ms) reported for previous single-cavity dual-comb solid-state lasers [14]. For free-running dual-comb fiber lasers, RF comb linewidths below 250 Hz have been reported [55–57]. Although a β-separation line analysis would provide more insights into the different noise sources contributing to the linewidth of these lasers, the reported results already indicate the extremely high mutual coherence that is achievable with fiber-based dual-combs. Since the frequency stability of dual-combs can be significantly improved in the post-processing, it is however only necessary to ensure that the relative noise between the combs is low enough to employ digital phase correction algorithms [28,58,59]. For that purpose, it is sufficient to keep the RF comb linewidth below half of the repetition rate difference on a $1/\Delta f_{\text{rep}}$ time scale, a condition which is easily met by our system.

6. Conclusion

We have demonstrated a diode-pumped single-cavity Yb:KYW dual-comb oscillator based on polarization multiplexing combined with a Yb-doped fiber amplifier optimized for minimal pulse broadening. The two sub-systems exhibit a high synergy since the emission wavelength of this as-yet unexplored gain crystal for dual-comb modelocking is close to the gain peak of the Yb-doped fiber amplifier. Further, the amplification process increases the limited output power of the single-mode diode-pumped solid-state laser by more than one order of magnitude to >1 W per comb. The careful design of the amplifier system together with the short length of the active fiber ensures that the temporal pulse broadening remains low so that after a simple grating compressor the pulses can be compressed to sub-90-fs pulses. No pre-chirping or other dispersion management is needed except for the grating compressor, which provides around -20’000 fs^2 GDD.

A thorough characterization of the intensity noise properties of the system shows that after the amplification process the RIN qualitatively follows the pump noise of the amplifier at low frequencies, while at higher frequencies the RIN of the oscillator becomes the main noise source as expected from theoretical predictions [46,47]. By stabilizing the power of the oscillator’s pump with a dedicated feedback loop, we could thus reduce the RIN of the amplified signal at the intersection between the noise frequencies dominated by the oscillator RIN and the frequencies within the bandwidth of the feedback loop. The substantial power of the seed laser enables a low noise floor of -155 dBc/Hz even after amplification.

A measurement of the timing noise of the two pulse trains revealed that the amplified signal inherits the timing noise properties of the solid-state oscillator. The proposed hybrid approach thus benefits from the advantages of fiber amplifier systems while preserving the low-noise characteristics supported by solid-state laser oscillators, and thereby gets the best from both worlds. Meanwhile, the system stays simple and does not require any active cooling. The proposed hybrid solution can be applied to other bulk dual-laser configurations, for example different gain crystals or spatial multiplexing [14].

A detailed study of the relative frequency fluctuations revealed a FWHM comb linewidth of around 700 Hz over a measurement duration of 100 ms. We attribute this ultra-low noise performance to the single-cavity solid-state laser architecture which proved valuable for mitigating noise spikes at low frequencies, in combination with the low-noise single-mode pump diode. By using computational phase correction in the post-processing, the frequency stability could be increased even further.

Our results show that MOPA based dual-comb sources using solid-state dual-comb modelocked lasers for seeding are a promising alternative to conventional fiber-oscillator-based systems, offering higher repetition rates, simpler amplification setups, lower high-frequency RIN, and the potential for lower phase noise as discussed in [24].

Funding. H2020 European Research Council (966718); Schweizerischer Nationalfonds zur Förderung der Wissenschaftlichen Forschung (40B1-0_203709, 40B2-0_180933); Innosuisse - Schweizerische Agentur für Innovationsförderung (40B1-0_203709, 40B2-0_180933).

Acknowledgments. We thank Dr. Valentin Wittwer and Prof. Dr. Thomas Südmeyer from Université de Neuchâtel for lending the ORION 1064 nm Laser Module.

Disclosures. The authors declare no conflicts of interest.

Data availability. Data underlying the results presented in this paper are available in [60].

References

1. H. R. Telle, G. Steinmeyer, A. E. Dunlop, J. Stenger, D. H. Sutter, and U. Keller, "Carrier-envelope offset phase control: A novel concept for absolute optical frequency measurement and ultrashort pulse generation," Appl. Phys. B: Lasers Opt. **69**(4), 327–332 (1999).
2. A. Apolonski, A. Poppe, G. Tempea, C. Spielmann, T. Udem, R. Holzwarth, T. W. Hänsch, and F. Krausz, "Controlling the Phase Evolution of Few-Cycle Light Pulses," Phys. Rev. Lett. **85**(4), 740–743 (2000).
3. D. J. Jones, S. A. Diddams, J. K. Ranka, A. Stentz, R. S. Windeler, J. L. Hall, and S. T. Cundiff, "Carrier-Envelope Phase Control of Femtosecond Mode-Locked Lasers and Direct Optical Frequency Synthesis," Science **288**(5466), 635–639 (2000).
4. T. Fortier and E. Baumann, "20 years of developments in optical frequency comb technology and applications," Commun. Phys. **2**(1), 153–168 (2019).
5. S. Schiller, "Spectrometry with frequency combs," Opt. Lett. **27**(9), 766–768 (2002).
6. Z. Chen, M. Yan, T. W. Hänsch, and N. Picqué, "A phase-stable dual-comb interferometer," Nat. Commun. **9**(1), 3035–3041 (2018).
7. I. Coddington, N. R. Newbury, and W. C. Swann, "Dual-comb spectroscopy," Optica **3**(4), 414–426 (2016).
8. I. Coddington, W. C. Swann, and N. R. Newbury, "Coherent Multiheterodyne Spectroscopy Using Stabilized Optical Frequency Combs," Phys. Rev. Lett. **100**(1), 013902 (2008).
9. I. Coddington, W. C. Swann, L. Nenadovic, and N. R. Newbury, "Rapid and precise absolute distance measurements at long range," Nat. Photonics **3**(6), 351–356 (2009).
10. E. Hase, T. Minamikawa, T. Mizuno, S. Miyamoto, R. Ichikawa, Y.-D. Hsieh, K. Shibuya, K. Sato, Y. Nakajima, A. Asahara, K. Minoshima, Y. Mizutani, T. Iwata, H. Yamamoto, and T. Yasui, "Scan-less confocal phase imaging based on dual-comb microscopy," Optica **5**(5), 634–643 (2018).
11. X. Yang, K. Xu, J. Yin, Y. Dai, F. Yin, J. Li, H. Lu, T. Liu, and Y. Ji, "Optical frequency comb based multi-band microwave frequency conversion for satellite applications," Opt. Express **22**(1), 869–877 (2014).
12. A. M. Zolot, F. R. Giorgetta, E. Baumann, J. W. Nicholson, W. C. Swann, I. Coddington, and N. R. Newbury, "Direct-comb molecular spectroscopy with accurate, resolved comb teeth over 43 THz," Opt. Lett. **37**(4), 638–640 (2012).
13. S. M. Link, A. Klenner, M. Mangold, C. A. Zaugg, M. Golling, B. W. Tilma, and U. Keller, "Dual-comb modelocked laser," Opt. Express **23**(5), 5521–5531 (2015).
14. J. Pupeikis, B. Willenberg, S. L. Camenzind, A. Benayad, P. Camy, C. R. Phillips, and U. Keller, "Spatially multiplexed single-cavity dual-comb laser," Optica **9**(7), 713–716 (2022).
15. T. Ideguchi, T. Nakamura, Y. Kobayashi, and K. Goda, "Kerr-lens mode-locked bidirectional dual-comb ring laser for broadband dual-comb spectroscopy," Optica **3**(7), 748–753 (2016).
16. S. Mehravar, R. A. Norwood, N. Peyghambarian, and K. Kieu, "Real-time dual-comb spectroscopy with a free-running bidirectionally mode-locked fiber laser," Appl. Phys. Lett. **108**(23), 231104–231109 (2016).
17. S. M. Link, D. J. H. C. Maas, D. Waldburger, and U. Keller, "Dual-comb spectroscopy of water vapor with a free-running semiconductor disk laser," Science **356**(6343), 1164–1168 (2017).
18. N. R. Newbury, I. Coddington, and W. Swann, "Sensitivity of coherent dual-comb spectroscopy," Opt. Express **18**(8), 7929–7945 (2010).
19. H. A. Haus and A. Mecozzi, "Noise of mode-locked lasers," IEEE J. Quantum Electron. **29**(3), 983–996 (1993).
20. Rüdiger Paschotta, Harald R. Telle, and U. Keller, "Noise of Solid-State Lasers," in *Solid-State Lasers and Applications*, A. Sennaroglu, ed. (CRC Press, 2007), pp. 473–510.
21. R. Paschotta, A. Schlatter, S. C. Zeller, H. R. Telle, and U. Keller, "Optical phase noise and carrier-envelope offset noise of mode-locked lasers," Appl. Phys. B **82**(2), 265–273 (2006).
22. U. Keller, "Intensity Noise and Timing Jitter of Modelocked Lasers," in *Ultrafast Lasers: A Comprehensive Introduction to Fundamental Principles with Practical Applications* (Springer International Publishing, 2021), pp. 589–637.
23. A. J. Benedick, J. G. Fujimoto, and F. X. Kärtner, "Optical flywheels with attosecond jitter," Nat. Photonics **6**(2), 97–100 (2012).
24. M. Endo, T. D. Shoji, and T. R. Schibli, "Ultralow Noise Optical Frequency Combs," IEEE J. Select. Topics Quantum Electron. **24**(5), 1–13 (2018).

25. M. Kowalczyk, Ł. Sterczewski, X. Zhang, V. Petrov, Z. Wang, and J. Sotor, "Dual-Comb Femtosecond Solid-State Laser with Inherent Polarization-Multiplexing," Laser Photonics Rev. **15**, 2000441 (2021).
26. S. L. Camenzind, D. Koenen, B. Willenberg, J. Pupeikis, C. R. Phillips, and U. Keller, "Timing jitter characterization of free-running dual-comb laser with sub-attosecond resolution using optical heterodyne detection," Opt. Express **30**(4), 5075–5094 (2022).
27. J. Pupeikis, B. Willenberg, F. Bruno, M. Hettich, A. Nussbaum-Lapping, M. Golling, C. P. Bauer, S. L. Camenzind, A. Benayad, P. Camy, B. Audoin, C. R. Phillips, and U. Keller, "Picosecond ultrasonics with a free-running dual-comb laser," Opt. Express **29**(22), 35735–35754 (2021).
28. C. R. Phillips, B. Willenberg, A. Nussbaum-Lapping, F. Callegari, S. L. Camenzind, J. Pupeikis, and U. Keller, "Coherently averaged dual-comb spectroscopy with a low-noise and high-power free-running gigahertz dual-comb laser," arXiv arXiv:2211.01368 (2022).
29. B. Willenberg, J. Pupeikis, L. M. Krüger, F. Koch, C. R. Phillips, and U. Keller, "Femtosecond dual-comb Yb:CaF_2 laser from a single free-running polarization-multiplexed cavity for optical sampling applications," Opt. Express **28**(20), 30275–30288 (2020).
30. A. Ruehl, A. Marcinkevicius, M. E. Fermann, and I. Hartl, "80 W, 120 fs Yb-fiber frequency comb," Opt. Lett. **35**(18), 3015–3017 (2010).
31. X. Li, M. A. R. Reber, C. Corder, Y. Chen, P. Zhao, and T. K. Allison, "High-power ultrafast Yb:fiber laser frequency combs using commercially available components and basic fiber tools," Rev. Sci. Instrum. **87**(9), 093114 (2016).
32. V. Shumakova, V. F. Pecile, J. Fellinger, M. Leskowschek, P. E. C. Aldia, A. S. Mayer, L. W. Perner, S. Salman, M. Fan, P. Balla, S. Schilt, C. M. Heyl, I. Hartl, G. Porat, and O. H. Heckl, "Spectrally tunable high-power Yb:fiber chirped-pulse amplifier," Photon. Res. **10**, 2309–2316 (2022).
33. T. Flöry, V. Stummer, J. Pupeikis, B. Willenberg, A. Nussbaum-Lapping, F. V. A. Camargo, M. Barkauskas, C. R. Phillips, U. Keller, G. Cerullo, A. Pugzlys, and A. Baltuska, "Rapid-scan nonlinear time-resolved spectroscopy over arbitrary delay intervals," arXiv arXiv:2211.12211 (2022).
34. N. V. Kuleshov, A. A. Lagatsky, A. V. Podlipensky, V. P. Mikhailov, and G. Huber, "Pulsed laser operation of Yb-doped $KY(WO_4)_2$ and $KGd(WO_4)_2$," Opt. Lett. **22**(17), 1317–1319 (1997).
35. N. V. Kuleshov, A. A. Lagatsky, V. G. Shcherbitsky, V. P. Mikhailov, E. Heumann, T. Jensen, A. Diening, and G. Huber, "CW laser performance of Yb and Er,Yb doped tungstates," Appl. Phys. B: Lasers Opt. **64**(4), 409–413 (1997).
36. H. Liu, J. Nees, and G. Mourou, "Diode-pumped Kerr-lens mode-locked Yb:$KY(WO_4)_2$ laser," Opt. Lett. **26**(21), 1723–1725 (2001).
37. S. Pekarek, C. Fiebig, M. C. Stumpf, A. E. H. Oehler, K. Paschke, G. Erbert, T. Südmeyer, and U. Keller, "Diode-pumped gigahertz femtosecond Yb:KGW laser with a peak power of 3.9 kW," Opt. Express **18**(16), 16320–16326 (2010).
38. Z. Zhang, C. Gu, J. Sun, C. Wang, T. Gardiner, and D. T. Reid, "Asynchronous midinfrared ultrafast optical parametric oscillator for dual-comb spectroscopy," Opt. Lett. **37**(2), 187–189 (2012).
39. A. Klenner, M. Golling, and U. Keller, "A gigahertz multimode-diode-pumped Yb:KGW enables a strong frequency comb offset beat signal," Opt. Express **21**(8), 10351–10357 (2013).
40. C. Li, N. Krauß, G. Schäfer, L. Ebner, O. Kliebisch, J. Schmidt, S. Winnerl, M. Hettich, and T. Dekorsy, "High-speed asynchronous optical sampling based on GHz Yb:KYW oscillators," Opt. Express **25**(8), 9204–9212 (2017).
41. U. Keller, K. J. Weingarten, F. X. Kärtner, D. Kopf, B. Braun, I. D. Jung, R. Fluck, R. Fluck, C. Honninger, N. Matuschek, N. aus der Au, and J. Dekorsy, "Semiconductor saturable absorber mirrors (SESAM's) for femtosecond to nanosecond pulse generation in solid-state lasers," IEEE J. Select. Topics Quantum Electron. **2**(3), 435–453 (1996).
42. F. X. Kärtner, I. D. Jung, and U. Keller, "Soliton mode-locking with saturable absorbers," IEEE J. Select. Topics Quantum Electron. **2**(3), 540–556 (1996).
43. D. J. Kane and R. Trebino, "Characterization of arbitrary femtosecond pulses using frequency-resolved optical gating," IEEE J. Quantum Electron. **29**(2), 571–579 (1993).
44. R. Trebino, K. W. DeLong, D. N. Fittinghoff, J. N. Sweetser, M. A. Krumbügel, B. A. Richman, and D. J. Kane, "Measuring ultrashort laser pulses in the time-frequency domain using frequency-resolved optical gating," Rev. Sci. Instrum. **68**(9), 3277–3295 (1997).
45. U. Keller, "Laser Rate Equations, Steady-State Solutions, Relaxation Oscillations, and Transfer Functions," in *Ultrafast Lasers: A Comprehensive Introduction to Fundamental Principles with Practical Applications* (Springer International Publishing, 2021), pp. 185–224.
46. M. Tröbs, P. Weßels, and C. Fallnich, "Power- and frequency-noise characteristics of an Yb-doped fiber amplifier and actuators for stabilization," Opt. Express **13**(6), 2224–2235 (2005).
47. H. Tünnermann, J. Neumann, D. Kracht, and P. Weßels, "Gain dynamics and refractive index changes in fiber amplifiers: a frequency domain approach," Opt. Express **20**(12), 13539–13550 (2012).
48. L. Nugent-Glandorf, T. A. Johnson, Y. Kobayashi, and S. A. Diddams, "Impact of dispersion on amplitude and frequency noise in a Yb-fiber laser comb," Opt. Lett. **36**(9), 1578–1580 (2011).
49. A. S. Mayer, W. Grosinger, J. Fellinger, G. Winkler, L. W. Perner, S. Droste, S. H. Salman, C. Li, C. M. Heyl, I. Hartl, and O. H. Heckl, "Flexible all-PM NALM Yb:fiber laser design for frequency comb applications: operation regimes and their noise properties," Opt. Express **28**(13), 18946–18968 (2020).

Optics EXPRESS

50. T. D. Shoji, W. Xie, K. L. Silverman, A. Feldman, T. Harvey, R. P. Mirin, and T. R. Schibli, "Ultra-low-noise monolithic mode-locked solid-state laser," Optica **3**(9), 995–998 (2016).
51. R. Paschotta, "Noise of mode-locked lasers (Part II): timing jitter and other fluctuations," Appl. Phys. B **79**(2), 163–173 (2004).
52. H. Shi, Y. Song, F. Liang, L. Xu, M. Hu, and C. Wang, "Effect of timing jitter on time-of-flight distance measurements using dual femtosecond lasers," Opt. Express **23**(11), 14057–14069 (2015).
53. K. Kieu and M. Mansuripur, "All-fiber bidirectional passively mode-locked ring laser," Opt. Lett. **33**(1), 64–66 (2008).
54. G. Di Domenico, S. Schilt, and P. Thomann, "Simple approach to the relation between laser frequency noise and laser line shape," Appl. Opt. **49**(25), 4801–4807 (2010).
55. H. Tian, R. Li, T. Endo, T. Kato, A. Asahara, L. A. Sterczewski, and K. Minoshima, "Dual-comb spectroscopy using free-running mechanical sharing dual-comb fiber lasers," Appl. Phys. Lett. **121**(21), 211104 (2022).
56. X. Zhao, G. Hu, B. Zhao, C. Li, Y. Pan, Y. Liu, T. Yasui, and Z. Zheng, "Picometer-resolution dual-comb spectroscopy with a free-running fiber laser," Opt. Express **24**(19), 21833–21845 (2016).
57. Y. Nakajima, Y. Hata, and K. Minoshima, "High-coherence ultra-broadband bidirectional dual-comb fiber laser," Opt. Express **27**(5), 5931–5944 (2019).
58. N. B. Hébert, V. Michaud-Belleau, J. Deschênes, and J. Genest, "Self-Correction Limits in Dual-Comb Interferometry," IEEE J. Quantum Electron. **55**(4), 1–11 (2019).
59. Ł. A. Sterczewski, A. Przewłoka, W. Kaszub, and J. Sotor, "Computational Doppler-limited dual-comb spectroscopy with a free-running all-fiber laser," APL Photonics **4**(11), 116102 (2019).
60. S. L. Camenzind, T. Sevim, B. Willenberg, J. Pupeikis, A. Nussbaum-Lapping, C. R. Phillips, and U. Keller, Data for "Free-running Yb:KYW dual-comb oscillator in a MOPA architecture", ETH Zurich Research Collection (2023), https://doi.org/10.3929/ethz-b-000597085.